

Low Delay Rate Allocation in WLANs Using Aggregation

Francesco Gringoli, Douglas J. Leith

Abstract—In this paper we consider transport layer approaches for achieving high rate, low delay communication over edge paths where the bottleneck is a modern WLAN which can aggregate multiple packets into each WLAN frame. We show that regulating send rate so as to maintain a target aggregation level can be used to avoid queue buildup at the WLAN AP. We derive an approximate downlink throughput model for WLANs using aggregation, verify its accuracy using experimental measurements, and using this determine a convex rate region. This allows us to derive a low delay proportional fair rate allocation for which we present a prototype transport layer implementation.

1 INTRODUCTION

While much attention in 5G has been focussed on the physical and link layers, it is increasingly being realised that a wider redesign of network protocols is also needed in order to meet 5G requirements. Transport protocols are of particular relevance for end-to-end performance, including end-to-end latency. For example, ETSI has recently set up a working group to study next generation protocols for 5G [1]. The requirement for major upgrades to current transport protocols is also reflected in initiatives such as Google QUIC [2], Coded TCP [3] and the Open Fast Path Alliance [4].

In this paper we consider next generation edge transport architectures of the type illustrated in Figure 1. Traffic to and from client stations is routed via a proxy located close to the network edge (e.g. within a cloudlet). This creates the freedom to implement new transport layer behaviour over the path between proxy and clients, which in particular includes the last wireless hop. One great advantage of this architecture is its ease of rollout since the new transport can be implemented as an app on the clients and no changes are required to existing servers.

Our interest is in achieving high rate, low delay communication. One of the most challenging requirements in 5G is the provision of connections with low end-to-end latency. In most use cases the target is for <100ms latency, while for some applications it is <10ms [5, Table 1]. In part, this reflects the fact that low delay is already coming to the fore in network services. For example, Amazon estimates that a 100ms increase in delay reduces its revenue by 1% [6], Google measured a 0.74% drop in web searches when delay was artificially increased by 400ms [7] while Bing saw a 1.2% reduction in per-user revenue when the service delay was increased by 500ms [8]. But the requirement for low latency also reflects the needs of next generation applications such as augmented reality and the tactile internet.

In the present paper we focus on situations where the last hop in Figure 1 is a modern WLAN and is the bot-

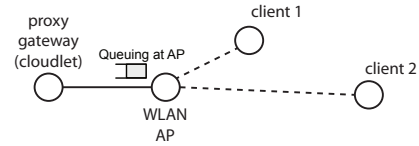


Fig. 1. Schematic of a cloudlet-based edge transport architecture. The bottleneck lies in WLAN hop so that queueing of downlink packets occurs at the AP (indicated on schematic).

tleneck. The transmission delay of a packet sent over the downlink is composed of two main components: (i) queueing delay at the AP and (ii) MAC contention time. The MAC contention time is determined by the WLAN contention mechanism and typically small, so the main challenge is to regulate the queueing delay. Key to our work is the ubiquity of aggregation in modern WLANs, a feature that brings goodput near to line-rate by reducing the relative time spent in accessing the channel when transmitting several packets to the same destination. Intuitively, the level of aggregation achieved is coupled to queueing. Namely, when only a few packets are queued then there are not enough to allow large aggregated frames to be assembled for transmission. Conversely, when there is a persistent queue backlog then there is a plentiful supply of packets and large frames can be consistently assembled. We show that regulating the send rate to a station so as to maintain an appropriate fixed aggregation level can be used to realise high rate, low delay communication. We then extend consideration to multiple stations. This requires characterising the rate region of WLANs with aggregation, which is highly non-trivial due to the strong coupling between aggregation and queueing. We develop an approximate model, verify its accuracy using experimental measurements and use this to derive a low-delay rate region for WLANs with aggregation. Fortunately, this low delay region is convex and so standard utility-fair optimisation approaches can be used to derive a low delay proportional fair rate allocation. We show how this rate allocation can be implemented at the transport layer and evaluate performance inside the ns-3 discrete event simulator and in an experimental testbed located in

- F. Gringoli is with University of Brescia, Italy.
- D. J. Leith is with Trinity College Dublin, Ireland. DL was supported by Science Foundation Ireland under Grant No. 13/RC/2077.

a realistic office radio environment.

In summary, our main contributions are as follows: (i) we establish that regulating send rate so as to maintain a target aggregation level can be used to realise high rate, low delay communication over modern WLANs; (ii) we derive a low delay rate region, show that it is convex and derive the low delay proportional fair rate allocation; (iii) we present a prototype transport layer implementation of this low delay rate allocation and evaluate its performance inside ns-3 and in a realistic office radio environment.

The rest of the paper is organized as follows. In Section 1.1 we review the related work, then Section 2 introduces notation and discusses measurement of the aggregation level in 802.11 frames and Section 3 introduces the general feedback algorithm which is proposed for regulating aggregation level, and so AP queueing delay. Section 4 derives a simplified model of aggregation and this is then used in Section 5 to derive the structure of the proportional fair rate allocation subject to a constraint on aggregation level. Section 6 describes how this proportional fair rate allocation can be implemented via the proposed feedback algorithm and presents simulation results and experimental measurements evaluating performance. The assumptions used in the analysis are reviewed in Section 7 and scope for their relaxation discussed. The paper conclusions are then summarised in Section 8.

1.1 Related Work

In recent years there has been an upsurge in interest in userspace transports due to their flexibility and support for innovation combined with ease of rollout. This has been greatly facilitated by the high efficiency possible in userspace with the support of modern kernels. Notable examples of new transports developed in this way include Google QUIC [2], UDT [9] and Coded TCP [3], [10], [11]. ETSI has also recently set up a working group to study next generation protocols for 5G [1]. The use of performance enhancing proxies, including in the context of WLANs, is also not new e.g. RFC3135 [12] provides an entry point into this literature. However, none of these exploit the use of aggregation in WLANs to achieve high rate, low delay communication.

Interest in using aggregation in WLANs pre-dates the development of the 802.11n standard in 2009 but has primarily focused on analysis and design for wireless efficiency, managing loss etc. For a recent survey see for example [13]. The literature on throughput modelling of WLANs is extensive but much of it focuses on so-called saturated operation, where transmitters always have a packet to send, see for example [14] for early work on saturated throughput modelling of 802.11n with aggregation. When stations are not saturated (so-called finite-load operation) then for WLANs which use aggregation (802.11n and later) most studies resort to the use of simulations to evaluate performance due to the complex interaction between arrivals, queueing and aggregation with CSMA/CA service. Notable exceptions include [15], [16] which adopt a bulk service queueing model that assumes a fixed, constant level of aggregation and [17] which extends the finite load approach of [18] for 802.11a/b/g but again assumes a fixed level of aggregation.

n	number of WLAN stations
N_{max}	maximum packets per frame
$N_{i,f}$	number of packets in frame f sent to station i
N_ϵ	target aggregation level
Δ	slot duration
$\mathcal{T}_{i,k}$	set of frames transmitted to station i in slot kl
T_{oh}	time used by MAC and PHY framing plus transmission of ACK
$T_{acc,j,f}$	airtime used for CSMA/CA contention transmitting frame f to station j
$\delta_{i,f}$	the time between transmission of frame $f+1$ and frame f
L	packet length in bits
$R_{i,f}$	PHY rate used to transmit the payload of frame f to station i
x_i	packet send rate to station i
K	feedback gain

TABLE 1

'Summary of main symbols used

Similarly, while utility fair optimisation has previously been considered for WLANs, e.g. [19], [20], [21] this has either ignored aggregation or confined consideration to solutions where only full-sized frames are transmitted (since this maximises throughput when there is freedom to adjust the transmission attempt probability, e.g. see [20] which considers use of TXOP bursting rather than frame aggregation but this just changes the overhead calculations involved).

2 PRELIMINARIES

2.1 Notation

\mathbf{x} denotes a vector and x_i the i 'th element of the vector. Superscript \bar{x} denotes $\log x$. μ_N denotes the expected value $E[N]$ of random variable N . The main symbols used are summarised in Table 1.

2.2 Aggregation in 802.11n, 802.11ac etc

A feature shared by all new WLAN standards since around 2009 (when 802.11n was introduced) has been the use of aggregation to amortise PHY and MAC framing overheads across multiple packets. This is essential for achieving high throughputs. Since PHY overheads are largely of fixed duration, increasing data rates reduces the time spent transmitting the frame payload but leaves the PHY overhead unchanged. Hence, the efficiency, as measured by the ratio of the time spent transmitting user data to the time spent transmitting an 802.11 frame, decreases as data rates increase unless the frame payload is also increased i.e. several user packets are aggregated and transmitted in a single frame.

Since the packets aggregated in a frame share the same destination station (at least in current 802.11 standards), aggregation effectively requires that per station queueing be used at the WLAN access point. When few packets are queued then there are insufficient packets available to allow large aggregated frames to be assembled for transmission. While the scheduler might delay transmission in anticipation of more packets arriving it is known that this is generally not advantageous, e.g. see [14], and we see no evidence of this in our experimental measurements. When the network is lightly loaded then such delay merely increases latency, while as the network load increases queue

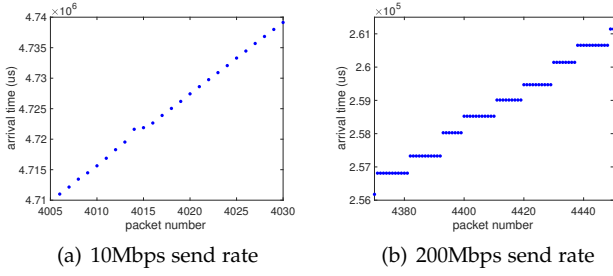


Fig. 2. Illustrating timestamp measurements for UDP packets transmitted over an 802.11ac downlink via aggregated frames to two client stations. The same downlink send rate us for for both client stations. Data is shown for one of the client stations.

backlogs start to develop and the level of aggregation naturally increases [14].

2.3 Measuring Aggregation

The level of aggregation can be readily measured at a receiver using packet timestamps. Namely, a timestamp is typically added by the NIC to each packet recording the time when it is received. When a frame carrying multiple packets is received then those packets have the same timestamp and so this can be used to infer which packets were sent in the same frame. For example, Figure 2 shows measured packet timestamps for two different downlink send rates. The setup consists of Linux server (running Debian Jessie) sending UDP packets using iperf 2.0.5 to two Linux clients (running Debian Stretch and with Broadcom BCM4360 802.11ac NICs) via an Asus RT-AC86U Access Point (which uses a Broadcom 4366E chipset). This setup allows high spatial usage (we observe that almost always three spatial streams are used) and high data rates (up to MCS 9). Note that unless otherwise stated we also use this same setup when presenting experimental measurements in the rest of this paper. It can be seen from Figure 2(a) that when the UDP arrival rate at the AP is relatively low each received packet has a distinct timestamp whereas at higher arrival rates, see Figure 2(b), packets start to be received in bursts having the same timestamp. This behaviour reflects the use by the AP of aggregation at higher arrival rates, as confirmed by inspection of the radio headers in the corresponding tcpdump data.

We note that lost packets may be retransmitted in a dedicated frame in which case the aggregation level of that frame is often lower than for regular frames, e.g. see Figure 3. Losses also mean that the number of received packets in a frame is lower than the number transmitted. Fortunately, by inserting a unique sequence number into the payload of each packet we can infer both losses and retransmissions since they respectively appear as “holes” in the received stream of sequence numbers and as out of order delivery. We can therefore adjust our book-keeping to compensate for them when estimating the aggregation level..

3 LOW DELAY OPERATION

To provide high rate, low latency communication for next generation 5G services we would like to select a downlink

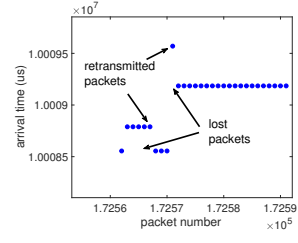


Fig. 3. Illustrating impact of packet loss on timestamp measurements for UDP packets transmitted via aggregated frames. In the first frame a burst of five packets are not received and are retransmitted in the second frame. In the third frame the first packet is lost and retransmitted by itself in the fourth frame. Two stations, 200Mbps downlink send rate to both, 802.11ac.

send rate which is as high as possible yet ensures that a persistent queue backlog does not develop at the AP. While measurements of round-trip time might be used to estimate the onset of queueing and adjust the send rate, it is known that this can be inaccurate when there is queueing in the reverse path. Accurately measuring one-way delay is also known in general to be challenging¹. In contrast, the number of packets aggregated in a frame is relatively easy to measure accurately and reliably at the receiver, as already noted.

3.1 Inferring Queueing From Level of Aggregation

Intuitively, the level of aggregation used in downlink transmissions to a station is coupled to the queue backlog at the AP of packets destined to the station. When few packets are queued then there are insufficient packets available to allow large aggregated frames to be assembled for transmission. Conversely, when the queue is persistently large then packets are available to be aggregated into large frames. This behaviour can, for example, be seen in the experimental measurements shown in Figure 4. Figure 4(a) shows a time history of number of packets aggregated in each frame and the mean one-way delay² experienced by packets sharing the same frame. It can be seen that the delay rises for frames 1000-2500 and that there is a corresponding increase in the number of packets aggregated in these frames to the maximum permitted value of $N_{max} = 64$. Figure 4(b) shows the same data, replotted as aggregation level vs delay. Although the relationship is a noisy one, it can be seen that the aggregation level indeed tends to rise with the delay until it hits the maximum allowed value.

3.2 Controlling Delay

The above observation motivates us to explore whether queueing delay at the AP can be controlled by regulating the

1. The impact of clock offset and skew between sender and receiver applies to all network paths. In addition, when a wireless hop is the bottleneck then the transmission delay can also change significantly over time depending on the number of active stations e.g. if a single station is active and then a second station starts transmitting the time between transmission opportunities for the original station may double.

2. Sender and receiver clocks are synchronised using NTP and we confirmed that clock skew between devices is minor over the duration of the experiment. One way delay is measured by sender inserting the current time into the packet payload immediately before making a socket call to transmit the packet, the receiver then compares this time with the time when the packet is received by the kernel.

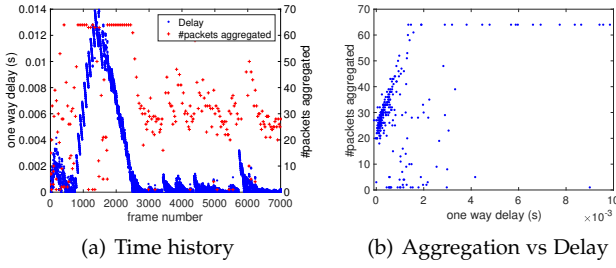


Fig. 4. Measured queueing delay and frame aggregation. Single downlink flow 400Mbps, 802.11ac

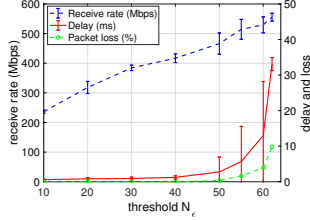


Fig. 5. Measured rate, delay and loss vs target aggregation level N_ϵ . $K = 1$, $\Delta = 1000ms$, 802.11ac with $N_{max} = 64$. Each data point summarises 250s of measurements.

packet arrival rate into the AP so as to maintain a specified level of aggregation.

We proceed by introducing a simple feedback loop to adjust the sender transmit rate (corresponding to the AP arrival rate, assuming no losses between sender and AP). Namely, time is partitioned into slots of duration Δ seconds and we let $\mathcal{T}_{i,k}$ denote the set of frames transmitted to station i in slot k . Station i measures the number of packets $N_{i,f}$ aggregated in frame f and reports the average $\hat{\mu}_{N_i}(k) := \frac{1}{|\mathcal{T}_{i,k}|} \sum_{f \in \mathcal{T}_{i,k}} N_{i,f}$ back to the sender. The sender then uses proportional feedback to increase its transmit rate x_i if the observed aggregation level $\hat{\mu}_{N_i}(k)$ is less than the target value N_ϵ and decrease it if $\hat{\mu}_{N_i}(k) > N_\epsilon$. This can be implemented using the pseudo-code shown in Algorithm 1. The stability of this feedback loop is analysed in Section 6.1.1.

Algorithm 1 Feedback loop adjusting transmit rate to regulate aggregation level.

```

k = 1
while 1 do
     $\hat{\mu}_{N_i} \leftarrow \frac{1}{|\mathcal{T}_{i,k}|} \sum_{f \in \mathcal{T}_{i,k}} N_{i,f}$ 
     $x_i \leftarrow x_i - K(\hat{\mu}_{N_i} - N_\epsilon)$ 
    k ← k + 1
end while

```

We implemented this feedback loop in the testbed setup described in Section 2 and Figure 5 shows experimental measurements of the client station receive rate (i.e. after any packet loss), one-way delay and packet loss (measured at the transport layer, so after any link layer retransmissions) as the target aggregation level N_ϵ is varied. Also shown are error bars indicating one standard deviation. Note that losses due to decoding errors were always recovered by retransmissions at the link-layer, thus packet loss is asso-

ciated only with queue overflow within the AP. It can be seen that, as expected, for aggregation levels close to the upper limit $N_{max} = 64$ the delay and loss rise rapidly with N_ϵ . However, when the aggregation is regulated to a lower level, less than about 40 packets, the delay is consistently low and there are no queue overflow losses.

Observe also in Figure 5 that the receive rate increases roughly linearly with N_ϵ . Recall that the rate is regulated to maintain the target aggregation level N_ϵ . Recall that service of the AP queue is stochastic in nature due to the random nature of the contention process used in 802.11 and we can expect this to induce a fluctuating queue backlog and so influence the aggregation level. Further, while iperf 2.0.5 uses packet pacing, this is only approximate and the packet transmissions are still somewhat bursty. Hence, it is perhaps unsurprising that a lower rate is required in order to maintain a lower aggregation level. For N_ϵ around 30 or 40, which as already noted ensures low delay, the rate is around 80% of the maximum.

4 WLAN CAPACITY WITH AGGREGATION

The results in Section 3 indicate that it is indeed possible to ensure high-rate, low delay operation. However, when transmitting to multiple stations then we have to jointly select the transmit rates to all of the stations since wireless is a shared medium. Further, many combinations of transmit rates can all yield low delay. Hence, to proceed we need to characterise the downlink rate region.

4.1 Modelling Aggregation

Consider downlink transmissions in a WLAN (so no collisions) with n client stations indexed by $i = 1, 2, \dots, n$. Index the packets arriving at the AP for transmission to station i by $k = 1, 2, \dots$ and let $\Delta_{i,k}$ denote the inter-arrival time between packet $k - 1$ and packet k . Recall that we control the packet sender (the proxy gateway in Figure 1) and so for simplicity we assume that this uses packet pacing, in which case the packet inter-arrival times at the AP are constant, i.e. $\Delta_{i,k} = \Delta_i$. Hence, $x_i = 1/\Delta_i$ is the rate in packets/sec at which packets arrive at the AP for transmission to station i and we let $\mathbf{x} = (x_1, \dots, x_n)^T$ denote the vector of station arrival rates. Packets are transmitted to station i by the AP within 802.11 frames. Index these frames by $f = 1, 2, \dots$ and let $\mathcal{F}_{i,f} \subset \{1, 2, \dots\}$ denote the set of packets aggregated within frame f transmitted to station i , $N_{i,f} = |\mathcal{F}_{i,f}|$ the number of packets aggregated and $\delta_{i,f}$ the time between transmission of frame $f - 1$ and frame f . Since a minimum of one packet must be contained within a frame and a maximum of N_{max} (typically 32 or 64) then $1 \leq N_{i,f} \leq N_{max}$. The setup is illustrated in Figure 6.

Suppose, for simplicity, that all packets are of length L bits (this can be easily relaxed). The airtime used by frame f transmitted to station i is then given by

$$T_{air,i,f} := T_{oh} + \frac{L}{R_{i,f}} N_{i,f} \quad (1)$$

where $R_{i,f}$ is the PHY rate used to transmit the payload of the frame and T_{oh} is the combined time used by MAC and PHY framing plus transmission of the ACK by the receiver.

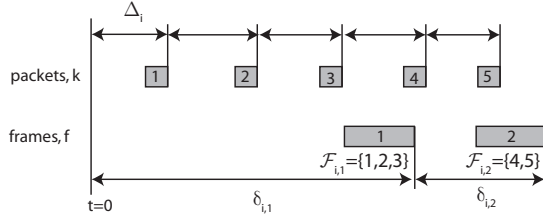


Fig. 6. Illustrating notation used for packet and frame timing. Packets arriving at the AP for transmission to station i are indexed $k = 1, 2, \dots$ with the time between packet $k - 1$ and packet k being Δ_i . Frames transmitted by the AP to station i are indexed $f = 1, 2, \dots$ with the time between frame $f - 1$ and frame f being $\delta_{i,f}$ and $\mathcal{F}_{i,f}$ the set of packets aggregated in frame f .

Assuming the AP transmits frames to stations in a round-robin fashion then

$$\delta_{i,f} = \sum_{j=1}^n T_{acc,j,f} + T_{oh} + \frac{L}{R_{j,f}} N_{j,f} \quad (2)$$

where $T_{acc,j,f}$ is airtime used for CSMA/CA contention by the AP when transmitting frame f to station j . Assume $N_{i,f}$ and $R_{i,f}$ are independent and vary in an i.i.d. manner across frames³. We also have that $T_{acc,j,f}$ is i.i.d by virtue of the 802.11 MAC operation since we consider the downlink only and so there are no collisions. Then taking expectations with respect to the 802.11 MAC and channel randomness,

$$\mu_{\delta_i} = \sum_{j=1}^n T_{acc} + T_{oh} + \frac{L}{\mu_{R_j}} \mu_{N_j} \quad (3)$$

where $\mu_{\delta_i} = E[\delta_{i,f}]$, $T_{acc} = E[T_{acc,j,f}]$ is the mean airtime per frame used for MAC contention, $\mu_{N_i} = E[N_{i,f}]$ is the average number of packets transmitted per frame and $\mu_{R_i} := 1/E[\frac{1}{R_{i,f}}]$ (note that in general⁴ $E[\frac{1}{R_{i,f}}] \neq 1/E[R_{i,f}]$). We can rewrite (3) equivalently in vector form

$$\mu_{\delta_i} = c + \mathbf{w}^T \boldsymbol{\mu}_N \quad (4)$$

where $c = n(T_{acc} + T_{oh})$, $\boldsymbol{\mu}_N = (\mu_{N_1}, \dots, \mu_{N_n})^T$, $\mathbf{w} = (\frac{L}{\mu_{R_1}}, \dots, \frac{L}{\mu_{R_n}})^T$.

To model the aggregation behaviour we proceed as follows. During interval $\delta_{i,f}$ we have $\delta_{i,f}/\Delta_i = \delta_{i,f}x_i$ packets arriving at the AP, ignoring quantisation effects for the moment. These packets are buffered in a queue until they can be transmitted. Letting $q_{i,f}$ denote the queue occupancy at the time when frame f is transmitted then $q_{i,f} = [q_{i,f-1} + \delta_{i,f}x_i - N_{i,f}]^+$. It is reasonable to suppose that the AP aggregates as many as possible of these packets

3. Variations in $N_{i,f}$ across frames arise due to fluctuations in the time $\delta_{i,f}$ between transmission opportunities as a result of the stochastic nature of the 802.11 MAC (when the time $\delta_{i,f}$ is longer then it is likely that more packets have arrived and $N_{i,f}$ is larger, conversely $N_{i,f}$ tends to be smaller when $\delta_{i,f}$ is shorter). Variations in PHY rate $R_{i,f}$ primarily arise due to channel fluctuations. Hence, assuming independence of $N_{i,f}$ and $R_{i,f}$ seems reasonable and is also consistent with our experimental measurements. Assuming that the $N_{i,f}$, $f = 1, \dots$ are i.i.d. is reasonable since the contention times $T_{acc,j,f}$ are i.i.d. Similarly, provided channel variations are i.i.d then it is reasonable to assume the $R_{i,f}$, $f = 1, \dots$ are i.i.d.

4. Indeed, to first-order $E[\frac{1}{R_{i,f}}] \approx \frac{1}{E[R_{i,f}]} + \frac{\text{Var}(R_{i,f})}{E[R_{i,f}]^3}$

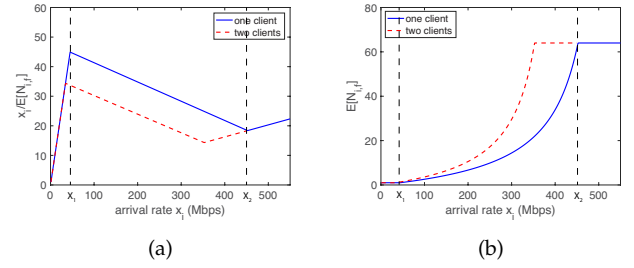


Fig. 7. Model predictions for UDP packets transmitted over an 802.11ac downlink to client stations. Data is shown for one and two client stations, the same send rate being used to all stations and indicated on the x-axes of the plots. Plot (a) shows x_i/μ_{N_i} and plot (b) μ_{N_i} vs send rate x_i . For a single client station, at arrival rate X_1 multiple packets start to be aggregated into each frame and at rate X_2 the upper limit N_{max} on the number of packets that can be aggregated in a frame is reached. 802.11ac MAC parameter values used.

queued for transmission into the next frame f , in which case $N_{i,f} = \min\{q_{i,f-1} + \delta_{i,f}x_i, N_{max}\}$ and

$$q_{i,f} = [q_{i,f-1} + \delta_{i,f}x_i - \min\{q_{i,f-1} + \delta_{i,f}x_i, N_{max}\}]^+ \quad (5)$$

$$= [q_{i,f-1} + \delta_{i,f}x_i - N_{max}]^+ \quad (6)$$

There are three operating regimes to consider. Firstly, when $E[\delta_{i,f}x_i] > N_{max}$ then this queue is unstable, the queue occupancy grows and so $N_{i,f} = N_{max}$ eventually for all frames f . Secondly, our main interest is in the regime where the queue backlog remains low i.e. $\delta_{i,f}x_i < N_{max}$ and the queue is cleared by each frame transmission so $q_{i,f} = 0$ and $N_{i,f} = \delta_{i,f}x_i$. Thirdly, there is the transition regime between regimes one and two where $E[\delta_{i,f}x_i] < N_{max}$ but $\delta_{i,f}x_i$ may sometimes be greater than N_{max} and $q_{i,f}$ may be non-zero. To simplify the analysis we assume that this third regime can be lumped with regime two⁵. Taking expectations we then have that

$$\mu_{N_i} = \Pi \circ \mu_{\delta_i} x_i = \Pi \circ (c + \mathbf{w}^T \boldsymbol{\mu}_N) x_i, \quad i = 1, \dots, n \quad (7)$$

where operator $\Pi \circ z$ projects z onto the interval $[1, N_{max}]$ i.e. $\Pi \circ z = \max\{1, \min\{N_{max}, z\}\}$. This gives n equations in n unknowns μ_{N_i} , $i = 1, \dots, n$ that we can solve to estimate the μ_{N_i} . For example, when all stations have same MCS rate $\mu_{R_j} = \mu_R$ and arrival rate $x_j = x$, then by symmetry aggregation is the same at all stations $\mu_{N_i} = \mu_N$ and

$$\mu_N = \Pi \circ (c + n w \mu_N) x = \Pi \circ \frac{cx}{1 - n x w} \quad (8)$$

where $w := \frac{L \mu_N}{\mu_R}$. Note that $1 - n x w > 0$ is a necessary condition for the backlog of packets at the AP not to be persistently growing.

Figure 7 illustrates the aggregation behaviour predicted by this model using 802.11ac MAC parameter values similar to those in our experimental measurements below⁶ When

5. This amounts to assuming that fluctuations in $\delta_{i,f}$ are sufficiently small, which holds when the contention time $T_{acc,i,f}$ is small relative to the frame transmission time $T_{air,i,f}$. Note that for typical 802.11ac MAC parameter values, $T_{acc,i,f}$ lies in the interval $[0, 169]\mu s$ and $T_{air,i,f} \approx 1.6ms$ i.e. $T_{acc,i,f}$ is roughly an order of magnitude smaller than $T_{air,i,f}$.

6. $9\mu s$ slots, $CWmin = 15$, $DIFS = 34\mu s$ giving $T_{acc} \approx 106\mu s$; three streams, 80Mhz channel, short GI giving $T_{oh} \approx 108\mu s$ and $\mu_R \approx 513$ Mbps for station 1 and $\mu_R \approx 850$ Mps for station 2; $L = 1500B$ of which 1470B is useful payload, $N_{max} = 64$.

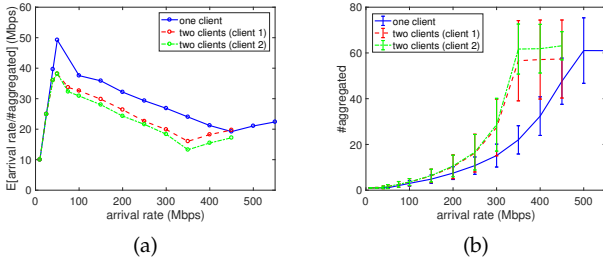


Fig. 8. Experimental measurements corresponding to the same setup as in Figure 7. Error bars are used in plot (b) to indicate the one standard deviation range of fluctuations in aggregation level N_i .

the arrival rate is low (below the rate marked X_1 in the figure), then only a single packet is transmitted in each frame, $\mu_{N_i} = 1$ and x_i/μ_{N_i} increases linearly with x_i . Once the arrival rate becomes sufficiently high then multiple packets are aggregated in each frame. The mean per packet overhead is $T_{oh}E[x_i/N_{i,f}|\mathbf{x}] \approx T_{oh}x_i/\mu_{N_i}$, and since x_i/μ_{N_i} decreases as rate x_i increases then the overhead also decreases. Eventually, as the arrival rate increases further still then the maximum aggregation limit N_{max} is reached and $x_i/\mu_{N_i} = x_i/64$ again increases linearly with x_i , albeit at a slower rate.

To help validate this model we collected experimental 802.11ac measurements of aggregation behaviour as the arrival rate and number of client stations is varied, see Figure 8. Comparing with Figure 7 it can be seen that the experimentally measured behaviour is qualitatively the same as the model, although the numerical values match up only approximately. The latter is to be expected since the real measurements include packet loss, a channel which is shared with other networks etc that are neglected by the model. Note that qualitative agreement is enough for our purposes since we are not going to use the model to make throughput predictions etc but instead to derive the structure of a utility fair rate allocation policy.

4.2 Analysis of Convexity

Ignoring, for the moment, the projection onto interval $[1, N_{max}]$, we can rewrite (7) as

$$\mu_N = (c + \mathbf{w}^T \mu_N) \mathbf{x} \quad (9)$$

Lemma 1 (Mean Frame Rate). *Let μ_N be a solution to (9) for arrival rates \mathbf{x} . Then $\frac{x_i}{\mu_{N_i}} = (1 - \mathbf{w}^T \mathbf{x})/c$ is a linear function of \mathbf{x} .*

Proof. From (9),

$$\frac{x_i}{\mu_{N_i}} = \frac{1}{c + \mathbf{w}^T \mu_N} \quad (10)$$

Also from (9),

$$\mathbf{w}^T \mu_N = (c + \mathbf{w}^T \mu_N) \mathbf{w}^T \mathbf{x} \quad (11)$$

Rearranging (11) yields

$$\mathbf{w}^T \mu_N = \frac{c \mathbf{w}^T \mathbf{x}}{1 - \mathbf{w}^T \mathbf{x}} \quad (12)$$

and substituting this into (10) we have

$$\frac{x_i}{\mu_{N_i}} = \frac{1}{c + \frac{c \mathbf{w}^T \mathbf{x}}{1 - \mathbf{w}^T \mathbf{x}}} = \frac{1 - \mathbf{w}^T \mathbf{x}}{c} \quad (13)$$

The claimed result now follows immediately. \square

Lemma 2 (Mean Aggregation Level). *Let μ_N be a solution to (9) for arrival rates \mathbf{x} . Then $\mu_N = \frac{c \mathbf{x}}{1 - \mathbf{w}^T \mathbf{x}}$. Further, μ_{N_i} , $i = 1, \dots, n$ is a convex function of $\tilde{\mathbf{x}} = (\log x_1, \dots, \log x_n)^T$ on the domain $\mathbf{w}^T e^{\tilde{\mathbf{x}}} < 1$.*

Proof. By Lemma 1, $\frac{x_i}{\mu_{N_i}} = \frac{1 - \mathbf{w}^T \mathbf{x}}{c}$. That is, $\mu_{N_i} = \frac{c x_i}{1 - \mathbf{w}^T \mathbf{x}}$, i.e.

$$\mu_N = \frac{c \mathbf{x}}{1 - \mathbf{w}^T \mathbf{x}} \quad (14)$$

as claimed. It can be verified by substituting this into (9) that it is indeed a solution.

Turning now to convexity, letting $\tilde{x}_i = \log x_i$ and $\tilde{\mu}_{N_i} = \log \mu_{N_i}$ then it follows from (7) that

$$\tilde{\mu}_{N_i} = \log c + \tilde{x}_i - \log(1 - \sum_{i=1}^n w_i e^{\tilde{x}_i}) \quad (15)$$

It can be verified by inspection of its first and second derivatives that $-\log(1 - z)$ is convex and increasing for $z < 1$ (the first derivative is $1/(1 - z)$ and the second $1/(1 - z)^2$). Since the exponential is convex we have that $\sum_{i=1}^n w_i e^{\tilde{x}_i}$ is a convex function of $\tilde{x}_1, \dots, \tilde{x}_n$. Composing these functions it follows from [22, p84] that $-\log(1 - \sum_{i=1}^n w_i e^{\tilde{x}_i})$ is convex in $\tilde{x}_1, \dots, \tilde{x}_n$ for $\mathbf{w}^T e^{\tilde{\mathbf{x}}} = \sum_{i=1}^n w_i e^{\tilde{x}_i} < 1$. The remaining terms in (15) are linear in $\tilde{x}_1, \dots, \tilde{x}_n$ and so convex, hence $\tilde{\mu}_{N_i}$ is a convex function of $\tilde{x}_1, \dots, \tilde{x}_n$. Now $\mu_{N_i} = e^{\tilde{\mu}_{N_i}}$ with e^z convex and increasing in z and $\tilde{\mu}_{N_i}$ is convex in $\tilde{\mathbf{x}}$. Hence, the composition $e^{\tilde{\mu}_{N_i}}$ of e^z with $\tilde{\mu}_{N_i}$ is also convex in $\tilde{\mathbf{x}}$ [22, p84]. That is, μ_{N_i} is convex in $\tilde{\mathbf{x}}$ as stated. \square

Now reinstating the constraint that μ_{N_i} must lie in the interval $[1, N_{max}]$, by Lemma 2 this can be enforced by projecting $\frac{c x_i}{1 - \mathbf{w}^T \mathbf{x}}$ onto this interval for each $i = 1, \dots, n$. Similarly, to constrain $\frac{x_i}{\mu_{N_i}}$ by Lemma 1 this can be enforced by projecting $(1 - \mathbf{w}^T \mathbf{x})/c$ onto interval $[x_i, \frac{x_i}{N_{max}}]$.

4.3 WLAN Downlink Rate Region

Stability of queue update (6) requires that for all stations $i = 1, \dots, n$ the mean arrival rate $E[\delta_{i,f} x_i]$ of packets into queue q_i is less than the maximum rate N_{max} at which packets are dequeued. Now $E[\delta_{i,f} x_i] = \mu_{\delta_i} x_i$, with μ_{δ_i} given by (3), and so by Lemma 2 for queue stability we require

$$\frac{c x_i}{1 - \mathbf{w}^T \mathbf{x}} < N_{max}, \quad i = 1, \dots, n \quad (16)$$

The set

$$\mathcal{R} = \{\mathbf{x} \in \mathbb{R}_+^n : \frac{c x_i}{1 - \mathbf{w}^T \mathbf{x}} < N_{max}, \quad i = 1, \dots, n\} \quad (17)$$

therefore contains the admissible packet arrival rates that can be supported while maintaining stable queues within the AP. Observe that $\frac{c x_i}{1 - \mathbf{w}^T \mathbf{x}} < N_{max}$ implies that $\frac{c \mathbf{w}^T \mathbf{x}}{1 - \mathbf{w}^T \mathbf{x}} \leq N_{max} \mathbf{w}^T \mathbf{1}$ i.e. $\mathbf{w}^T \mathbf{x} < N_{max} \mathbf{w}^T \mathbf{1} / (c + N_{max} \mathbf{w}^T \mathbf{1}) < 1$.

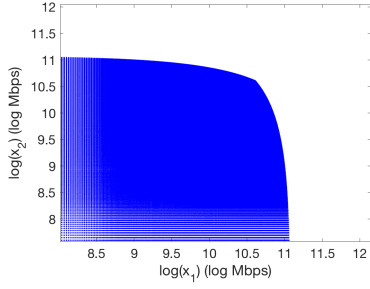


Fig. 9. Illustrating rate region $\tilde{\mathcal{R}}$ (for typical 802.11ac parameter values).

Hence, expressing set \mathcal{R} in terms of the transformed variable $\tilde{\mathbf{x}} = \log(\mathbf{x})$ yields set

$$\tilde{\mathcal{R}} = \{\tilde{\mathbf{x}} \in \mathbb{R}^n : \frac{ce^{\tilde{x}_i}}{1 - \mathbf{w}^T e^{\tilde{\mathbf{x}}}} < N_{max}, i = 1, \dots, n\} \quad (18)$$

which by Lemma 2 is convex. Rate region $\tilde{\mathcal{R}}$ is illustrated in Figure 9.

5 LOW DELAY FAIR RATE ALLOCATION

We now embed the foregoing rate and delay constraints within a utility optimisation with the aim of deriving a low-delay rate allocation algorithm suited to use by next generation edge transport protocols. We obtain the following optimisation P ,

$$\begin{aligned} \max_{\tilde{\mathbf{x}}} \sum_{i=1}^n U(e^{\tilde{x}_i}) \\ \text{s.t. } \mu_{N_i}(\tilde{\mathbf{x}}) \leq N_{\epsilon}, i = 1, \dots, n \end{aligned} \quad (19)$$

where $\tilde{x}_i = \log x_i$, $\mu_{N_i}(\tilde{\mathbf{x}}) = \frac{ce^{\tilde{x}_i}}{1 - \sum_{j=1}^n w_j e^{\tilde{x}_j}}$, design parameter $N_{\epsilon} < N_{max}$ and utility function $U(\cdot)$ is such that $U(e^z)$ is concave in z . Constraints (19) ensure low delay by preventing large queue backlogs from developing at the AP. The constraints are all convex and the utility is concave, hence optimisation P is convex. The Lagrangian is

$$L(\tilde{\mathbf{x}}, \lambda, \mu) = - \sum_{i=1}^n U(e^{\tilde{x}_i}) + \sum_{i=1}^n \lambda_i (\mu_{N_i}(\tilde{\mathbf{x}}) - N_{\epsilon}) \quad (20)$$

where $\lambda_i, i = 1, \dots, n$ are the multipliers.

5.1 Low Delay Proportional Fair Rate Allocation

In the important case where the utility function $U(\cdot)$ is the log, for which the solution of optimisation P correspond to the proportional fair rate allocation, then it turns out that we can explicitly characterise the solution.

Theorem 1 (Proportional Fair Rate Allocation). *The solution to optimisation P is $x_j = \alpha/w_j$ where scaling factor $\alpha = \frac{N_{\epsilon} w_{max}}{(c + N_{\epsilon} w_{max} n)} > 0$ with $w_{max} = \max_{i \in \{1, \dots, n\}} w_i$.*

Proof. Since the optimisation is convex the KKT conditions are necessary and sufficient for optimality. Namely, an optimum satisfies

$$\sum_{j=1}^n \lambda_j \frac{\partial \mu_{N_j}}{\partial \tilde{x}_i} = 1, i = 1, \dots, n \quad (21)$$

$$\lambda_i (\mu_{N_i}(\tilde{\mathbf{x}}) - N_{\epsilon}) = 0, i = 1, \dots, n \quad (22)$$

where $\mu_{N_i} = \frac{cx_i}{1 - \mathbf{w}^T \mathbf{x}}$ and $\frac{\partial \mu_{N_i}}{\partial \tilde{x}_i} = \frac{cx_i}{1 - \mathbf{w}^T \mathbf{x}} \left(1 + \frac{w_i x_i}{(1 - \mathbf{w}^T \mathbf{x})}\right)$, $\frac{\partial \mu_{N_j}}{\partial \tilde{x}_i} = \frac{cx_j w_i x_i}{(1 - \mathbf{w}^T \mathbf{x})^2}$. When $x_j = \alpha/w_j$ then

$$\sum_{j=1}^n \lambda_j \frac{\partial \mu_{N_j}}{\partial \tilde{x}_i} = \frac{c\alpha}{1 - n\alpha} \left(\frac{\lambda_i}{w_i} + \sum_{j=1}^n \frac{\lambda_j}{w_j} \frac{\alpha}{(1 - n\alpha)} \right) \quad (23)$$

and

$$\lambda_i (\mu_{N_i}(\tilde{\mathbf{x}}) - N_{\epsilon}) = \lambda_i \left(\frac{c\alpha/w_i}{1 - n\alpha} - N_{\epsilon} \right) \quad (24)$$

Selecting

$$\lambda_i/w_i = \begin{cases} \gamma := \frac{1}{c} \frac{(1-n\alpha)^2}{1-(n-n_{max})\alpha^2} & w_i = w_{max} \\ 0 & w_i < w_{max} \end{cases} \quad (25)$$

where $n_{max} = |\{i \in \{1, \dots, n\} : w_i = w_{max}\}| \geq 1$ is the number of stations with maximal w_i , then

$$\sum_{j=1}^n \lambda_j \frac{\partial \mu_{N_j}}{\partial \tilde{x}_i} = \gamma c \frac{1 - (n - n_{max})\alpha^2}{(1 - n\alpha)^2} = 1 \quad (26)$$

and so condition (21) is satisfied. Further, for the stated choice of α we have that $\frac{c\alpha/w_{max}}{1 - n\alpha} = N_{\epsilon}$. Hence $\lambda_i (\mu_{N_i}(\tilde{\mathbf{x}}) - N_{\epsilon}) = 0$ for all $i = 1, \dots, n$ and so by (24) complementary slackness condition (22) is also satisfied. The stated conclusion now follows. \square

Observe that the proportional fair rate allocation assigns a rate to station i that is proportional to its mean MCS/PHY rate μ_{R_i} since $1/w_i = \mu_{R_i}/L$. That is, stations with a better channel are allowed to send at a higher rate. Proportional fair rate allocations are not always equal airtime allocations, for example this is not the case in WLANs with MU-MIMO [21]. However, in the the present case this does indeed hold:

Corollary 1 (Equal Airtime). *The proportional fair rate allocation assigns equal mean per packet airtime to every client station.*

Proof. The mean per packet air time used by station i is given by $T_i = \frac{c}{n} \frac{x_i}{\mu_{N_j}} + w_i x_i$. Substituting the proportional fair solution from Theorem 1, $T_i = \frac{c}{n} \frac{\alpha}{w_i \mu_{N_j}} + \alpha$. By Lemma 2, $\mu_{N_i} = \frac{cx_i}{1 - \mathbf{w}^T \mathbf{x}}$ and using this in the expression for T_i and rearranging yields $T_i = 1/n$. This holds for all $i \in \{1, \dots, n\}$. \square

While the airtime used by each station is equal, stations with different channels operate with different aggregation levels, with transmissions on channels with a higher mean MCS/PHY rate having a higher aggregation level than transmissions on channels with a low MCS/PHY rate:

Corollary 2 (Different Aggregation Levels). *With a proportional fair rate allocation the mean aggregation level μ_{N_i} of transmissions to station i is proportional to the mean MCS/PHY rate μ_{R_i} , namely $\mu_{N_i} = \frac{c\alpha}{1 - n\alpha} \frac{\mu_{R_i}}{L}$.*

Proof. By Lemma 2, $\mu_{N_i} = \frac{cx_i}{1 - \mathbf{w}^T \mathbf{x}}$. Substituting the proportional fair solution from Theorem 1 it follows that $\mu_{N_i} = \frac{1}{w_i} \frac{c\alpha}{1 - n\alpha}$. Now recall that $1/w_i = \mu_{R_i}/L$. \square

As discussed in more detail in Section 6, the proportional lends itself to implementation using easily measured quantities.

5.2 Other Utility Functions

When the Slater condition is satisfied then strong duality holds and we can find an optimum by dual ascent,

$$\tilde{\mathbf{x}}(k+1) \in \arg \min_{\tilde{\mathbf{x}}} L(\tilde{\mathbf{x}}, \boldsymbol{\lambda}(k)) \quad (27)$$

$$\lambda_i(k+1) = [\lambda_i(k) + \alpha(\mu_{N_i}(\tilde{\mathbf{x}}(k)) - N_\epsilon)^+] \quad (28)$$

where $\alpha > 0$ is the step size. The Lagrangian is not separable since the expression for $\hat{\mu}_{N_i}$ is coupled to all of the arrival rates \tilde{x}_j , $j = 1, \dots, n$.

Let $\hat{\mu}_{N_i}(k)$ be the empirical average of the number of packets aggregated in the frames sent between dual updates k and $k+1$. Replace μ_{N_i} with $\hat{\mu}_{N_i}(k)$ in the update and note that $E[\hat{\mu}_{N_i}(k)|\tilde{\mathbf{x}}(k)] = \mu_{N_i}(\tilde{\mathbf{x}}(k))$ since the $N_{i,f}$ are assumed i.i.d given fixed arrival rate $\mathbf{x}(k)$. This yields the following approximate update,

$$\tilde{\mathbf{x}}(k+1) \in \arg \min_{\tilde{\mathbf{x}}} L(\tilde{\mathbf{x}}, \boldsymbol{\lambda}(k)) \quad (29)$$

$$= \arg \min_{\tilde{\mathbf{x}}} - \sum_{i=1}^n U(e^{\tilde{x}_i}) + \sum_{i=1}^n \lambda_i \hat{\mu}_{N_i}(\tilde{\mathbf{x}}) \quad (30)$$

$$\lambda_i(k+1) = [\lambda_i(k) + \alpha(\hat{\mu}_{N_i}(k) - N_\epsilon)^+] \quad (31)$$

Observe that by replacing $\mu_{N_i}(\tilde{\mathbf{x}}(k))$ by the observations $\hat{\mu}_{N_i}(k)$ we implicitly evaluate $\mu_{N_i}(\tilde{\mathbf{x}}(k)) = \frac{ce^{\tilde{x}_i}}{1 - \sum_{j=1}^n w_j e^{\tilde{x}_j}}$. By avoiding explicit evaluation we do not need to know the w_j parameter values, to guarantee convergence its enough that we know the relationship is convex. By construction we have $E[\hat{\mu}_{N_i}(k)|\tilde{\mathbf{x}}(k)] = \mu_{N_i}(\tilde{\mathbf{x}}(k))$. Applying Theorem 1 of [23], then this update will converge in expectation to a solution of the original problem..

6 PERFORMANCE EVALUATION

To evaluate performance we first tested the controlling algorithm inside the discrete event simulator ns-3; we then ported the code on a Linux node transmitting to wireless stations located in an office environment. We introduce in the next paragraph details common to the two implementations while we report specific results later.

6.1 Prototype Implementation

We build on the simple feedback loop in Algorithm 1. Time is partitioned into slots of duration Δ seconds and $\mathcal{T}_{i,k}$ denotes the set of frames transmitted to station i in slot k . Client stations measure⁷ $N_{i,f}$ and $R_{i,f}$ and at the end of each slot report the averages $\hat{\mu}_{N_i}(k) := \frac{1}{|\mathcal{T}_{i,k}|} \sum_{f \in \mathcal{T}_{i,k}} N_{i,f}$ and $\hat{\mu}_{R_i}(k) := \frac{1}{|\mathcal{T}_{i,k}|} \sum_{f \in \mathcal{T}_{i,k}} R_{i,f}$ back to a server (in the payload of a UDP packet) which then uses this information to select the downlink send rates \mathbf{x} to the clients. Recall that we are considering next generation edge transports and so this server would typically be located in the cloud close to the network edge. While it may be located on the wireless access point this is not essential, and indeed we demonstrate this feature in all of our experiments by making use of a proprietary closed access point. This software architecture is illustrated in Figure 10.

7. Note that the proportional fair rate allocation ensures that the send rate to every station is non-zero i.e. no station is starved, see Theorem 1. Hence each station always receives packets and is able to estimate $\hat{\mu}_{N_i}(k)$ and $\hat{\mu}_{R_i}(k)$.

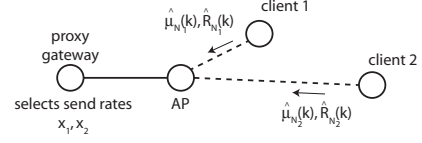


Fig. 10. Schematic of scheduler architecture. Clients send reports of observed aggregation level and MCS rate to proxy which then uses this information to adjust the downlink send rate to each station.

The server uses a proportional feedback loop to adjust the vector of downlink send rates \mathbf{x} . Namely, it increases the rate x_{i^*} of the station i^* with highest MCS rate $\hat{\mu}_{R_i}(k)$ when its observed aggregation level $\hat{\mu}_{N_i}(k)$ is less than the target value N_ϵ and decreases x_{i^*} when $\hat{\mu}_{N_i}(k) > N_\epsilon$, i.e. at slot k

$$x_{i^*}(k+1) = x_{i^*}(k) - K(\hat{\mu}_{N_i}(k) - N_\epsilon) \quad (32)$$

where feedback gain K is a design parameter. The rates of the other stations are then assigned proportionally,

$$x_i(k+1) = x_{i^*}(k+1) \frac{\hat{\mu}_{R_j}}{\hat{\mu}_{R_{i^*}}}, \quad i = 1, \dots, n \quad (33)$$

Pseudo code for this update is shown in Algorithm 2.

Algorithm 2 Pseudo code for proportional fair rate controller

```

k = 1
while 1 do
     $\hat{\mu}_{N_i} \leftarrow \frac{1}{|\mathcal{T}_{i,k}|} \sum_{f \in \mathcal{T}_{i,k}} N_{i,f}$ ,  $\hat{\mu}_{R_i} \leftarrow \frac{1}{|\mathcal{T}_{i,k}|} \sum_{f \in \mathcal{T}_{i,k}} R_{i,f}$ 
     $i^* \in \arg \max_{i \in \{1, \dots, n\}} w_i$ 
     $x_{i^*} \leftarrow x_{i^*} - K(\hat{\mu}_{N_{i^*}} - N_\epsilon)$ 
     $x_j \leftarrow x_{i^*} \frac{\hat{\mu}_{R_j}}{\hat{\mu}_{R_{i^*}}}$ ,  $j = 1, \dots, n$ 
    k ← k + 1
end while

```

Note that this update only uses readily available observations. Namely, the frame aggregation level $N_{i,f}$ and the MCS rate $R_{i,f}$, both of which can be observed in userspace by packet sniffing on client i . While we relied on a model to establish convexity and the form of the low delay proportional fair rate allocation, no model parameters are needed in order to actually implement Algorithm 2 (apart from the number of stations n that the server allocates rates to, which is known trivially). Design parameters N_ϵ , gain K and update interval Δ do need to be selected. Selection of target aggregation level N_ϵ has already been discussed in detail, with a typical value being $N_\epsilon = 32$, which leaves the feedback gain K and update interval Δ . We investigate these further below but typical values are $K = 1/n$ (where n is the number of client stations) and $\Delta = 500ms$ or $1000ms$.

6.1.1 Stability Analysis

Before proceeding we briefly comment on the stability of the nonlinear feedback loop :

$$x_i(k+1) = x_i(k) - K(\mu_{N_i}(k) - N_\epsilon) \quad (34)$$

where $\mu_{N_i}(k) = \Pi \circ (\frac{cx_i(k)}{1 - w^T \mathbf{x}(k)})$ by Lemma 2. Note that the actual feedback loop (32) in Algorithms 1 and 2 uses $\hat{\mu}_{N_i}(k)$ rather than $\mu_{N_i}(k)$, which introduces zero mean

noise but should not affect stability. Letting x_i^* denote the proportional fair rate for station i and $\mathbf{x}^* = (x_1^*, \dots, x_n^*)^T$ then

$$\left. \frac{\partial \mu_{N x_i}(k)}{\partial x_i(k)} \right|_{\mathbf{x}(k)=\mathbf{x}^*} = \frac{c}{(1 - \mathbf{w}^T \mathbf{x}^*)} \left(1 + \frac{w_i x_i^*}{(1 - \mathbf{w}^T \mathbf{x}^*)} \right) \quad (35)$$

and linearising the dynamics (34) about this point yields,

$$\delta x_i(k+1) \approx \left(1 - K \left. \frac{\partial \mu_{N x_i}(k)}{\partial x_i(k)} \right|_{\mathbf{x}(k)=\mathbf{x}^*} \right) \delta x_i(k) \quad (36)$$

where $\delta x_i(k) = x_i(k) - x_i^*$. For stability we require $0 < K \left. \frac{\partial \mu_{N x_i}(k)}{\partial x_i(k)} \right|_{\mathbf{x}(k)=\mathbf{x}^*} < 2$ [24]. Recall $w_i = L/\mu_{R_i}$, $c = n(T_{acc} + T_{oh})$ and $x_i^* = \alpha/w_i$ and so $1 - \mathbf{w}^T \mathbf{x}^* = 1 - N_\epsilon w_{max}/(T_{acc} + T_{oh} + N_\epsilon w_{max})$. Observe that c scales with n and so for stability we need to scale K as $1/n$ i.e. $K = K_0/n$. Typical values are $T_{acc} + T_{oh} > 200 \mu s$, $N_\epsilon = 32$, $L = 1500B$, $\mu_{R_i} > 100 Mbps$, $x_i^* = 8000$ packets per second giving $K_0 < 12$ for stability, and unless otherwise stated we use $K_0 = 1$ in the rest of the paper. Note that this only ensures local stability. While a necessary condition for global stability it is not sufficient and further analysis of the nonlinear dynamics is needed to confirm conditions on K to ensure global stability.

6.2 Measurements in a Simulated Environment

6.2.1 Modifications to ns-3

We implemented the controller as a new module in ns-3: based on the received feedbacks it periodically configures the sending rate of `udp-client` applications colocated at a single node connected to an Access Point. Each wireless station receives a single UDP traffic flow at a `udp-server` application that we modified to collect frame aggregation statistics and periodically transmit these to the controller at intervals of $\Delta = 500ms$. The controller uses feedback gain $K = 1/n$. We also developed a round-robin scheduler at the AP and added new functions to let stations determine the MCS of each received frame together with the number of MPDU packets it contains: we release the new code open-source⁸. In the following experiments we always use a 802.11ac physical layer operating over an 80MHz channel: we use VHT rates for data frames and legacy rates for control frames. As validation we reproduced a number of the experimental measurements using simulations, e.g. Fig 8, and found them to be in good agreement.

6.2.2 Simulated Scenarios and Results

We report in Fig. 11 (top) the aggregated application layer goodput and delay for an increasing number of receivers: each point in the figure averages results from 12 simulations with different seeds. For this experiment stations are located two meters away from the transmitting AP, datarate is fixed to MCS 9 and the Number of Spatial Streams (NSS) is set to 2; UDP datagrams contain 1470 bytes of payload, feedbacks contain 60 bytes of payload, and each AMPDU frame carries at most 64 packets. The upper red-star line is the theoretical limit: we computed it by taking into account AMPDU with

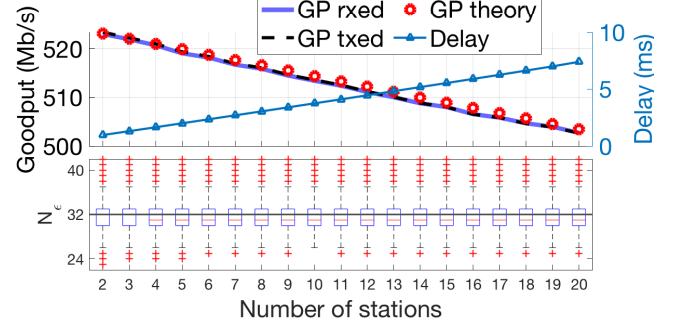


Fig. 11. Top figure: application layer GoodPut (GP) and delay for increasing number of receivers in a ns-3 simulated BSS with MCS = 9, NSS = 2. Bottom figure: boxplot of aggregation level N_ϵ .

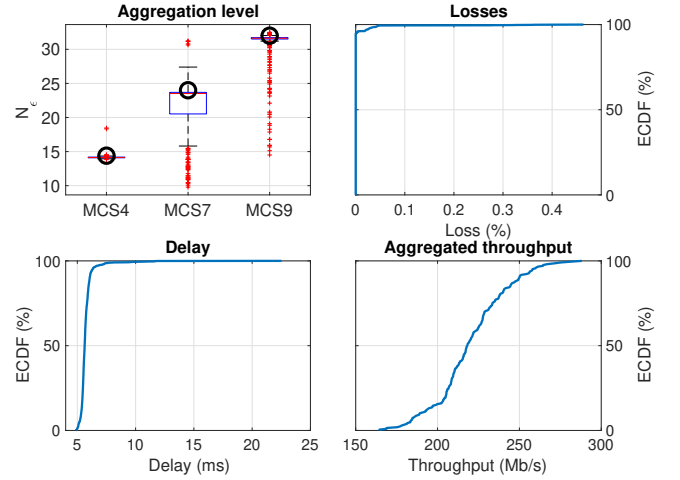


Fig. 12. Performance with 8 receivers placed randomly in a square of side 40m: MCS is chosen by MinstrelHT algorithm, NSS = 1.

$N_\epsilon = 32$ packets, 10 feedbacks per second per receiver, 10 beacons per second, and no collisions. The aggregated goodput measured at receivers (continuous line) is close to the theoretical limit with only a few Kb/s missing for 20 receivers, and it follows the configuration set by the controller (dashed line) that distributes resource equally between receivers: the measured Jain's Fairness Index is always 1. Average delay increases almost linearly at the rate of $350 \mu s$ per additional station while minimum delay is constant and equal to $60 \mu s$. We also report in Fig. 11 (bottom) statistics about N_ϵ . For each point we consider data from all receivers across the 12 simulations: edges of the boxes represent the 25th and 75th percentiles of the available data. Aggregation level is very close to the target 32 (grey horizontal line) and exhibits very small oscillations. In this experiment we did not observe losses.

We report in Fig. 12 performance for another scenario with 8 receivers placed randomly in a square of side 40m and the AP located in its center: we configured MinstrelHT algorithm as rate controller. This time we limit NSS to 1 to avoid excessive variability in the choice operated by the rate controller. We ran experiments until we collected 200 points where the rate controller converged to a stable choice for all receivers, i.e., with more than 85% of frames received with the same MCS. We group receivers by MCS and report statistics on N_ϵ for each group as boxplots in

⁸. We invite interested readers to request code by contacting the corresponding author.

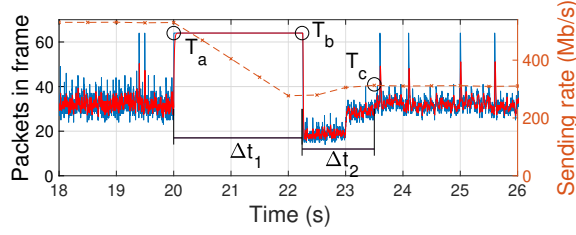


Fig. 13. Illustrating adaption of send rate by feedback algorithm in response to a change in channel conditions (from use of 2 spatial streams down to 1 spatial stream). Single client station, MCS 9

the top-left subfigure. We also show with a thick circle the expected choice for a proportional fair rate allocation that assigns equal airtime to all receivers which corresponds to smaller aggregates for lower MCS: experimental results perfectly match the analytical values. In clockwise order we then report the ECDF of losses, aggregated goodput and delay for the same dataset. Albeit negligible, losses appear in this configuration because of far away nodes not being able to correctly decode all packets; delay is slightly higher than in the previous scenario due to the slower datarates; and goodput can drop down to 150Mb/s when MinstrelHT selects MCS4 everywhere but converges to 300Mb/s with MCS 9 (theoretical maximum goodput with MCS 9, NSS 1 and $N_e = 32$ is 307Mb/s). Even though other MCS values can be selected, this happens only when MinstrelHT does not converge and keeps oscillating between different datarates so that we discard such experiments.

In Fig. 13 we illustrate how the algorithm reacts to channel changes. We start with 2 spatial streams, MCS 9 and at $t = T_a = 20\text{s}$ we switch to 1 spatial stream. For $\Delta t_1 = 2.24\text{s}$ all AMPDUs hit the maximum aggregation level of 64 packets and we start observing losses. During this time it can be seen that the algorithm, which updates the send rate twice per second ($\Delta = 500\text{ms}$), is slowing down the sending rate. It takes four rounds to reach a rate compatible with the channel, but it takes a little bit more to stabilise the aggregation level at the AP in $t = T_b$. After another three rounds (for approximately $\Delta t_2 = 1.26$) the sending rate settles at its new value in $t = T_c$.

6.3 Experimental Results in a Real Network

We next provide results that we captured with the hardware we already introduced in Section 2.3. We add remark here that we did not change anything at the driver layer, we only disabled AMSDU aggregation on the Asus AP. At every client we configured the BCM4360 wireless card in monitor mode so that we can run the software that measures delivery statistics through a raw socket and periodically transmits them back to the sender, transparently to the receiving iperf application. At the sender we use a modified version of iperf where we implemented the feedback collector and our controlling algorithm. We also briefly note that we repeated the following experiments with different chipsets at the AP (e.g., from QCA) and did not observe any major differences.

6.3.1 Tracking Changing Channel Conditions

We begin by presenting measurements in Figure 14 which demonstrate the ability of the feedback loop in Algorithm

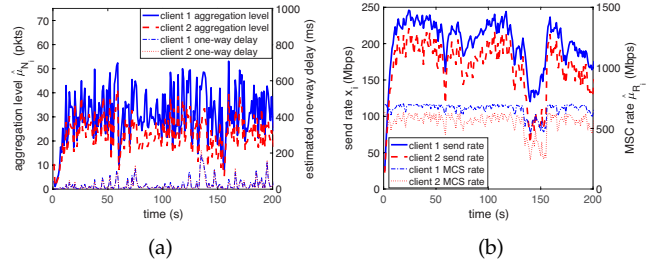


Fig. 14. Experimental measurements illustrating proportional fair rate allocation and adaptation to changing channel conditions to maintain roughly constant aggregation level and so low delay. Two client stations, 802.11ac, $N_e = 32$, $K = 1/n$, $\Delta = 1000\text{ms}$.

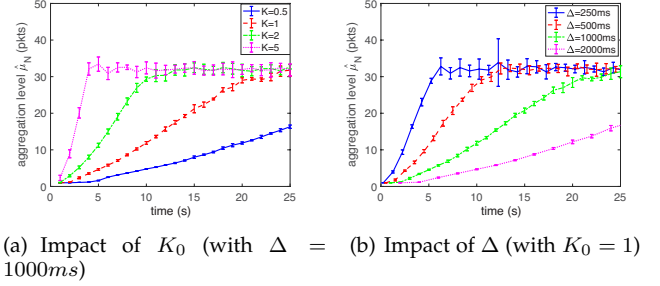


Fig. 15. Convergence rate vs feedback gain K_0 and update interval Δ . Mean and standard deviation from 10 runs at each parameter value. One client, 802.11ac, $N_e = 32$.

2 to adjust the rate allocation to reflect changing channel conditions so as to maintain both low delay and fairness. These measurements are taken during the day in an office environment where the unlicensed channels are shared by many networks and groups of people move about, creating a complex changing radio 5GHz environment (by taking additional measurements at night we confirmed that the channel is indeed stable when these factors are removed). These measurements have the advantage of showing real-world behaviour but at the cost of uncertainty as to the source of the observed channel fluctuations.

Station 1 is closer to the AP and so generally has a higher MCS rate than station 2. It can be seen from Figure 14(a) that the aggregation level of station 1 is regulated at around the target value of $N_e = 32$ packets, although there are fluctuations due to channel variations etc. It can be seen from Figure 14(b) that the send rates of the stations are roughly proportional to their MCS rates, corresponding to the proportional fair allocation. Adaptation of the send rates to changes in channel conditions is also evident, e.g. around time 140s there is a sharp decrease in the MCS rates of both stations (which we believe is due to movement of a group of people across the path between AP and clients). It can be seen from Figure 14(b) that the send rates adapt to this change in channel conditions, and from Figure 14(a) that, apart from a short spike in delay when the channel initially changes, the delay remains regulated at a low value despite the large changes in channel conditions.

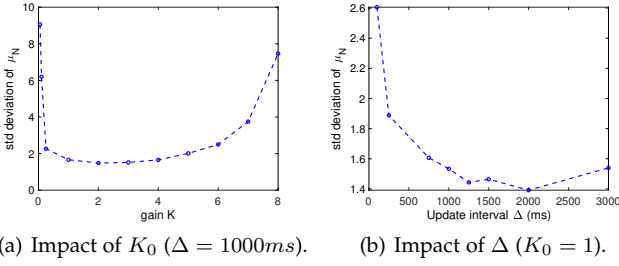


Fig. 16. Noise rejection (as measured by standard deviation of $\hat{\mu}_N$) vs feedback gain K_0 and update interval Δ . One client, 802.11ac.

6.3.2 Convergence Rate

We expect that the speed at which the aggregation level and send rate converge to their target values when a station first starts transmitting is affected by the choice of feedback gain $K = K_0/n$ and update interval Δ . Figure 15 plots measurements showing the transient following startup of a station vs the choice of K_0 and Δ . The plots show the average and standard deviation from 10 runs for each choice of parameter value.

It can be seen from Figure 15(a) that as gain K_0 is increased (while holding Δ fixed) the time to converge to the target aggregation level $N_e = 32$ decreases. However, as the gain is increased the feedback loop eventually becomes unstable. Indeed, not shown in the plot is the data for $K_0 = 10$ which shows large, sustained oscillations that would obscure the other data on the plot. Similarly, it can be seen from Figure 15(b) that as the update interval Δ is decreased the convergence time decreases.

6.3.3 Disturbance Rejection

Observe in Figure 15 that while the convergence time decreases as K_0 is increased the corresponding error bars indicated on the plots increase. As well as the convergence time we are also interested in how well the controller regulates the aggregation level about the target value N_e . Intuitively, when the gain K_0 is too low then the controller is slow to respond to changes in the channel and the aggregation level will thereby show large fluctuations. The situation when K_0 is increased increased we expect feedback loop is also able to respond more quickly to genuine changes in channel behaviour. However, when the gain is too high it may overreact and so magnify the fluctuations on aggregation level (with instability being an extreme instance of this, see Section 6.1.1). This behaviour can be seen in Figure 16(a) which plots measurements of the standard deviation of the aggregation level $\hat{\mu}_N$ (where the empirical mean is calculated over the update interval Δ of the feedback loop) as the control gain K_0 is varied.

When the the update interval Δ is made smaller we expect that the observations $\hat{\mu}_{N_i}(k)$ and $\hat{\mu}_{R_i}(k)$ will tend to become more noisy (since they are based on fewer frames) which may also tend to cause the aggregation level to fluctuate more. However, the feedback loop is also able to respond more quickly to genuine changes in channel behaviour. Conversely, as Δ increases the estimation noise falls but the feedback loop becomes more sluggish. Figure 16(b) plots measurements of the standard deviation of the

aggregation level $\hat{\mu}_N$ as Δ is varied. It can be seen that due to the interplay between these two effects that the standard deviation of $\hat{\mu}_N$ increases when Δ selected too small or too large, with a sweet spot for Δ around 1250-2000ms.

7 ASSUMPTIONS

In this section we review the assumptions used in our analysis, and in particular try to identify those assumptions that can be readily relaxed and those that cannot.

1) Downlink Only. We focus on the downlink, as is common in the wireless literature since it typically carries the bulk of traffic. Achieving low delay on the downlink is also the more challenging task for an edge transport since the queue at the AP cannot be directly observed. In contrast, on the uplink traffic shaping can be implemented at the client (e.g. within the app implementing the edge transport layer) thereby making the uplink queue occupancy visible to the transport layer. By communicating this to the proxy it can then jointly allocate client downlink and uplink rates to ensure low delay and high rate.

2) Link Layer Losses/Retransmissions Ignored. The theoretical analysis in Sections 4 and 5 ignores link layer losses and associated retransmissions to streamline the presentation, although of course our experimental measurements include these effects. It is straightforward to extend the analysis to include these by adjusting equation (7) to include retransmissions. The proportional fair solution remains an equal airtime one but the airtime now includes the time consumed by retransmissions.

3) WLAN is Bottleneck. We assume that the WLAN is the bottleneck. This is probably reasonable in enterprise edge networks or when the proxy server is co-located with the AP. However, when the proxy is located in the cloud then the bottleneck may well lie in the backhaul path between the AP and the proxy. Our initial measurements (which we plan to report on separately) indicate that observation of the aggregation level can be used to infer the bottleneck location i.e. WLAN or backhaul. This could be then used to restrict application of the approach in the present paper to situations where the WLAN is the bottleneck. That leaves open the question of how to achieve low delay and high rate when the backhaul is the bottleneck, but since this is a major undertaking in its own right we leave this as future work.

4) Centralised Operation. Algorithm 2 is centralised in nature, namely clients report measurements to the proxy which then decides on the appropriate downlink send rate for each client. This is a feature of the edge transport architecture considered here, providing the flexibility to create more flexible rate allocation approaches. Standard reformulations, e.g. ADMM or the approach in [23], might be used to solve optimisation P in a distributed fashion at the cost of increased complexity and slower convergence.

8 SUMMARY & CONCLUSIONS

In this paper we establish that regulating send rate so as to maintain a target aggregation level can be used to realise high rate, low delay communication over modern WLANs. Building on this, we derive an approximate throughput

model for WLANs with aggregation, use this to determine a convex low delay rate region and so obtain the low delay proportional fair rate allocation. We present a prototype transport layer implementation of this low delay rate allocation and evaluate its performance both within a simulated and in a realistic office radio environment.

REFERENCES

- [1] Next Generation Protocols – Market Drivers and Key Scenarios. European Telecommunications Standards Institute (ETSI), 2016. [Online]. Available: http://www.etsi.org/images/files/ETSIWhitePapers/etsi_wp17_Next_Generation_Protocols_v01.pdf
- [2] J. Iyengar and I. Swett, “QUIC: A UDP-Based Secure and Reliable Transport for HTTP/2,” IETF Internet Draft, 2015. [Online]. Available: <https://tools.ietf.org/html/draft-tsvwg-quic-protocol-00>
- [3] M. Kim, J. Cloud, A. ParandehGheibi, L. Urbina, K. Fouli, D. J. Leith, and M. Medard, “Congestion control for coded transport layers,” in *Proc IEEE International Conference on Communications (ICC)*, 2014, pp. 1228–1234.
- [4] Open Fast Path, 2016. [Online]. Available: <http://www.openfastpath.org/>
- [5] 5G White Paper. Next Generation Mobile Networks (NGMN) Alliance, 2015. [Online]. Available: https://www.ngmn.org/uploads/media/NGMN_5G_White_Paper_V1_0.pdf
- [6] T. Flach, N. Dukkupati, A. Terzis, B. Raghavan, N. Cardwell, Y. Cheng, A. Jain, S. Hao, E. Katz-Bassett, and R. Govindan, “Reducing web latency: the virtue of gentle aggression,” *ACM SIGCOMM Computer Communication Review*, vol. 43, no. 4, pp. 159–170, 2013.
- [7] W. Zhou, Q. Li, M. Caesar, and P. Godfrey, “ASAP: A low-latency transport layer,” in *Proceedings of the Seventh Conference on emerging Networking EXperiments and Technologies*. ACM, 2011, p. 20.
- [8] S. Souders, “Velocity and the bottom line,” in *Velocity (Web Performance and Operations Conference)*, 2009. [Online]. Available: <http://radar.oreilly.com/2009/07/velocity-making-your-site-fast.html>
- [9] Y. Gu and R. L. Grossman, “Udt: Udp-based data transfer for high-speed wide area networks,” *Comput. Netw.*, vol. 51, no. 7, pp. 1777–1799, May 2007. [Online]. Available: <http://dx.doi.org/10.1016/j.comnet.2006.11.009>
- [10] M. Karzand, D. J. Leith, J. Cloud, and M. Medard, “Design of FEC for Low Delay in 5G,” *IEEE Journal Selected Areas in Communications (JSAC)*, vol. 35, no. 8, pp. 1783–1793, 2016.
- [11] A. Garcia-Saavedra, M. Karzand, and D. J. Leith, “Low Delay Random Linear Coding and Scheduling Over Multiple Interfaces,” *IEEE Trans on Mobile Computing*, vol. 16, no. 11, pp. 3100–3114, 2017.
- [12] J. Border, M. Kojo, J. Griner, G. Montenegro, and Z. Shelby, “Performance enhancing proxies intended to mitigate link-related degradations,” *Internet Requests for Comments, RFC Editor, RFC* 3135, June 2001.
- [13] R. Karmakar, S. Chattopadhyay, and S. Chakraborty, “Impact of ieee 802.11n/ac phy/mac high throughput enhancements on transport and application protocols: A survey,” *IEEE Communications Surveys Tutorials*, vol. 19, no. 4, pp. 2050–2091, Fourthquarter 2017.
- [14] T. Li, Q. Ni, D. Malone, D. Leith, Y. Xiao, and T. Turletti, “Aggregation with Fragment Retransmission for Very High-Speed WLANs,” *IEEE/ACM Transactions on Networking*, vol. 17, no. 2, pp. 591–604, 2009.
- [15] S. Kuppa and G. Dattatreya, “Modeling and Analysis of Frame Aggregation in Unsaturated WLANs with Finite Buffer Stations,” in *Proc WCNC*, 2006, pp. 967–972.
- [16] B. Bellalta and M. Oliver, “A space-time batch-service queueing model for multi-user mimo communication systems,” in *Proceedings of the 12th ACM International Conference on Modeling, Analysis and Simulation of Wireless and Mobile Systems*, ser. MSWiM ’09. New York, NY, USA: ACM, 2009, pp. 357–364. [Online]. Available: <http://doi.acm.org/10.1145/1641804.1641866>
- [17] B. Kim, H. Hwang, and D. Sung, “Effect of Frame Aggregation on the Throughput Performance of IEEE 802.11n,” in *Proc WCNC*, 2008, pp. 1740–1744.
- [18] D. Malone, K. Duffy, and D. Leith, “Modeling the 802.11 distributed coordination function in nonsaturated heterogeneous conditions,” *IEEE/ACM Trans. Netw.*, vol. 15, no. 1, pp. 159–172, Feb. 2007. [Online]. Available: <http://dx.doi.org/10.1109/TNET.2006.890136>
- [19] A. Checco and D. J. Leith, “Proportional Fairness in 802.11 Wireless LANs,” *IEEE Communications Letters*, vol. 15, no. 8, pp. 807–809, August 2011.
- [20] —, “Fair Virtualization of 802.11 Networks,” *IEEE/ACM Trans. Netw.*, vol. 23, no. 1, pp. 148–160, Feb. 2015. [Online]. Available: <http://dx.doi.org/10.1109/TNET.2013.2293501>
- [21] V. Valls and D. Leith, “Proportional Fair MU-MIMO in 802.11 WLANs,” *Wireless Communications Letters, IEEE*, vol. 3, no. 2, pp. 221–224, 2014.
- [22] S. Boyd and L. Vandenberghe, *Convex Optimization*. New York, NY, USA: Cambridge University Press, 2004.
- [23] V. Valls and D. J. Leith, “A Convex Optimization Approach to Discrete Optimal Control,” *IEEE Transactions on Automatic Control*, 2018.
- [24] W. J. Rugh, *Linear System Theory*. Pearson, 1995.

PLACE
PHOTO
HERE

IEEE.

PLACE
PHOTO
HERE

Francesco Gringoli received the Laurea degree in telecommunications engineering from the University of Padua, Italy, in 1998 and the PhD degree in information engineering from the University of Brescia, Italy, in 2002. Since 2018 he is Associate Professor of Telecommunications at the Dept. of Information Engineering at the University of Brescia, Italy. His research interests include security assessment, performance evaluation and medium access control in Wireless LANs. He is a senior member of the

Doug Leith graduated from the University of Glasgow in 1986 and was awarded his PhD, also from the University of Glasgow, in 1989. In 2001, Prof. Leith moved to the National University of Ireland, Maynooth and then in Dec 2014 to Trinity College Dublin to take up the Chair of Computer Systems in the School of Computer Science and Statistics. His current research interests include wireless networks, network congestion control, distributed optimization and data privacy.